Mid-infrared waveguides in zinc sulfide crystal

Qiang An,[1] Yingying Ren,[1] Yuechen Jia,[1] Javier Rodríguez Vázquez de Aldana,[2] and Feng Chen[1,*]

[1]*School of Physics, State Key Laboratory of Crystal Materials and Key Laboratory of Particle Physics and Particle Irradiation, Ministry of Education, Shandong University, Jinan 250100, China*
[2]*Laser Microprocessing Group, Universidad de Salamanca, Salamanca 37008, Spain*
**drfchen@sdu.edu.cn*

Abstract: Depressed cladding optical waveguides have been fabricated in a zinc sulfide (ZnS) crystal by femtosecond laser inscription. The structures support single- or multi-mode guidance at the mid-infrared wavelength of ~4 μm. The two-dimensional refractive index profiles of the single-mode waveguides have been reconstructed, and the modal profiles of TE and TM modes were calculated numerically, that show very good agreement with the measured near-field modal profiles. The minimum propagation losses of the multimode cladding waveguides at 4 μm were ~1.1 dB/cm for the TE polarization and ~1.3 dB/cm for the TM polarization.

OCIS codes: (130.3060) Infrared; (230.7380) Waveguides, channeled; (130.3120) Integrated optics devices.

References and links

1. J. R. Meyer, C. A. Hoffman, F. J. Bartoli, and L. R. Ram-Mohan, "Type-II quantum-well lasers for the mid-wavelength infrared," Appl. Phys. Lett. **67**(6), 757–759 (1995).
2. I. Vurgaftman, J. R. Meyer, N. Tansu, and L. J. Mawst, "InP-Based Dilute-Nitride Mid-Infrared Type-II 'W' Quantum-Well Lasers," J. Appl. Phys. **96**(8), 4653–4655 (2004).
3. L. J. Mawst, J. Y. T. Huang, D. P. Xu, J. Y. Yeh, G. Tsvid, T. F. Kuech, and N. Tansu, "MOCVD grown Dilute-Nitride Type-II Quantum Wells," IEEE J. Sel. Top. Quantum Electron. **14**(4), 979–991 (2008).
4. N. Bandyopadhyay, Y. Bai, S. Tsao, S. Nida, S. Slivken, and M. Razeghi, "Room temperature continuous wave operation of λ : 3-3.2 μm quantum cascade lasers," Appl. Phys. Lett. **101**(24), 241110 (2012).
5. N. Bandyopadhyay, S. Slivken, Y. Bai, and M. Razeghi, "High power, continuous wave, room temperature operation of λ :3.4 μm and λ ~ 3.55μm InP-based quantum cascade lasers," Appl. Phys. Lett. **100**(21), 212104 (2012).
6. S.-S. Kim, C. Young, and B. Mizaikoff, "Miniaturized mid-infrared sensor technologies," Anal. Bioanal. Chem. **390**(1), 231–237 (2008).
7. G. Z. Mashanovich, M. M. Milošević, M. Nedeljkovic, N. Owens, B. Xiong, E. J. Teo, and Y. Hu, "Low loss silicon waveguides for the mid-infrared," Opt. Express **19**(8), 7112–7119 (2011).
8. M. M. Milošević, P. S. Matavulj, P. Yang, A. Bagolini, and G. Z. Mashanovich, "Rib waveguides for mid-infrared silicon photonics," J. Opt. Soc. Am. B **26**(9), 1760–1766 (2009).
9. A. J. Maker and A. M. Armani, "Low-loss silica-on-silicon waveguides," Opt. Lett. **36**(19), 3729–3731 (2011).
10. A. Ródenas, G. Martin, B. Arezki, N. Psaila, G. Jose, A. Jha, L. Labadie, P. Kern, A. Kar, and R. Thomson, "Three-dimensional mid-infrared photonic circuits in chalcogenide glass," Opt. Lett. **37**(3), 392–394 (2012).
11. Y. Tan, A. Rodenas, F. Chen, R. R. Thomson, A. K. Kar, D. Jaque, and Q. Lu, "70% slope efficiency from an ultrafast laser-written Nd:$GdVO_4$ channel waveguide laser," Opt. Express **18**(24), 24994–24999 (2010).
12. J. Siebenmorgen, K. Petermann, G. Huber, K. Rademaker, S. Nolte, and A. Tünnermann, "Femtosecond laser written stress-induced Nd:$Y_3Al_5O_{12}$ (Nd:YAG) channel waveguide laser," Appl. Phys. B **97**(2), 251–255 (2009).
13. T. Calmano, J. Siebenmorgen, O. Hellmig, K. Petermann, and G. Huber, "Nd:YAG waveguide laser with 1.3 W output power, fabricated by direct femtosecond laser writing," Appl. Phys. B **100**(1), 131–135 (2010).
14. A. Rodenas and A. K. Kar, "High-contrast step-index waveguides in borate nonlinear laser crystals by 3D laser writing," Opt. Express **19**(18), 17820–17833 (2011).
15. A. Benayas, W. F. Silva, A. Ródenas, C. Jacinto, J. Vázquez de Aldana, F. Chen, Y. Tan, R. R. Thomsom, N. D. Psaila, D. T. Reid, G. A. Torchia, A. K. Kar, and D. Jaque, "Ultrafast laser writing of optical waveguides in ceramic Yb:YAG: a study of thermal and non-thermal regimes," Appl. Phys., A Mater. Sci. Process. **104**(1), 301–309 (2011).
16. A. Ródenas, G. A. Torchia, G. Lifante, E. Cantelar, J. Lamela, F. Jaque, L. Roso, and D. Jaque, "Refractive index change mechanisms in femtosecond laser written ceramic Nd:YAG waveguides: micro-spectroscopy experiments and beam propagation calculations," Appl. Phys. B **95**(1), 85–96 (2009).
17. G. A. Torchia, A. Rodenas, A. Benayas, E. Cantelar, L. Roso, and D. Jaque, "Highly efficient laser action in femtosecond-written Nd:yttrium aluminum garnet ceramic waveguides," Appl. Phys. Lett. **92**(11), 111103 (2008).

#185234 - $15.00 USD Received 11 Feb 2013; revised 9 Mar 2013; accepted 9 Mar 2013; published 13 Mar 2013

18. N. Dong, Y. Yao, F. Chen, and J. R. Vazquez de Aldana, "Channel waveguides preserving luminescence features in Nd^{3+}:Y_2O_3 ceramics produced by ultrafast laser inscription," Phys. Status Solidi **5**(5–6), 184–186 (2011).
19. N. D. Psaila, R. R. Thomson, H. T. Bookey, A. K. Kar, N. Chiodo, R. Osellame, G. Cerullo, A. Jha, and S. Shen, "Er:Yb-doped oxyfluoride silicate glass waveguide amplifier fabricated using femtosecond laser inscription," Appl. Phys. Lett. **90**(13), 131102 (2007).
20. D. J. Little, M. Ams, P. Dekker, G. D. Marshall, J. M. Dawes, and M. J. Withford, "Femtosecond laser modification of fused silica: the effect of writing polarization on Si-O ring structure," Opt. Express **16**(24), 20029–20037 (2008).
21. D. G. Lancaster, S. Gross, H. Ebendorff-Heidepriem, K. Kuan, T. M. Monro, M. Ams, A. Fuerbach, and M. J. Withford, "Fifty percent internal slope efficiency femtosecond direct-written Tm^{3+}:ZBLAN waveguide laser," Opt. Lett. **36**(9), 1587–1589 (2011).
22. L. B. Fletcher, J. J. Witcher, N. Troy, S. T. Reis, R. K. Brow, and D. M. Krol, "Direct femtosecond laser waveguide writing inside zinc phosphate glass," Opt. Express **19**(9), 7929–7936 (2011).
23. A. Ródenas, G. A. Torchia, G. Lifante, E. Cantelar, J. Lamela, F. Jaque, L. Roso, and D. Jaque, "Refractive index change mechanisms in femtosecond laser written ceramic Nd:YAG waveguides: micro-spectroscopy experiments and beam propagation calculations," Appl. Phys. B **95**(1), 85–96 (2009).
24. V. Apostolopoulos, L. Laversenne, T. Colomb, C. Depeursinge, R. P. Salathé, M. Pollnau, R. Osellame, G. Cerullo, and P. Laporta, "Femtosecond irradiation induced refractive index changes and cannel waveguiding in bulk Ti^{3+}:Sapphire," Appl. Phys. Lett. **85**(7), 1122–1124 (2004).
25. J. Burghoff, S. Nolte, and A. Tünnermann, "Origins of waveguiding in femtosecond laser-structured $LiNbO_3$," Appl. Phys., A Mater. Sci. Process. **89**(1), 127–132 (2007).
26. A. G. Okhrimchuk, V. K. Mezentsev, V. V. Dvoyrin, A. S. Kurkov, E. M. Sholokhov, S. K. Turitsyn, A. V. Shestakov, and I. Bennion, "Waveguide-saturable absorber fabricated by femtosecond pulses in YAG:Cr^{4+} crystal for Q-switched operation of Yb-fiber laser," Opt. Lett. **34**(24), 3881–3883 (2009).
27. A. G. Okhrimchuk, A. V. Shestakov, I. Khrushchev, and J. Mitchell, "Depressed cladding, buried waveguide laser formed in a YAG:Nd^{3+} crystal by femtosecond laser writing," Opt. Lett. **30**(17), 2248–2250 (2005).
28. A. Benayas, W. F. Silva, C. Jacinto, E. Cantelar, J. Lamela, F. Jaque, J. R. Vázquez de Aldana, G. A. Torchia, L. Roso, A. A. Kaminskii, and D. Jaque, "Thermally resistant waveguides fabricated in Nd:YAG ceramics by crossing femtosecond damage filaments," Opt. Lett. **35**(3), 330–332 (2010).
29. Y. Ren, G. Brown, A. Ródenas, S. Beecher, F. Chen, and A. K. Kar, "Mid-infrared waveguide lasers in rare-earth-doped YAG," Opt. Lett. **37**(16), 3339–3341 (2012).
30. Y. Jia, F. Chen, and J. R. Vázquez de Aldana, "Efficient continuous-wave laser operation at 1064 nm in Nd:YVO_4 cladding waveguides produced by femtosecond laser inscription," Opt. Express **20**(15), 16801–16806 (2012).
31. Y. Jia, J. R. Vazquez de Aldana, C. Romero, Y. Ren, Q. Lu, and F. Chen, "Femtosecond-laser-inscribed BiB_3O_6 nonlinear cladding waveguide for second-harmonic generation," Appl. Phys. Express **5**(7), 072701 (2012).
32. N. Dong, F. Chen, and J. R. Vazquez de Aldana, "Efficient second harmonic generation by birefringent phase matching in femtosecond laser inscribed KTP cladding waveguides," Phys. Status Solidi **6**(7), 306–308 (2012).
33. J. Siebenmorgen, K. Petermann, G. Huber, K. Rademaker, S. Nolte, and A. Tunnermann, "Femtosecond laser written stress-induced Nd:$Y_3Al_5O_{12}$(Nd:YAG) channel waveguide laser," Appl. Phys. B **97**(2), 251–255 (2009).
34. http://www.ispoptics.com.
35. N. Huot, R. Stoian, A. Mermillod-Blondin, C. Mauclair, and E. Audouard, "Analysis of the effects of spherical aberration on ultrafast laser-induced refractive index variation in glass," Opt. Express **15**(19), 12395–12408 (2007).
36. RSoft Design Group, Computer Software BeamPROP, http://www.rsoftdesign.com.

1. Introduction

Since the emergence of type-II quantum well lasers (based on GaSb and dilute-nitride semiconductors) and InP-based quantum cascade lasers [1–5], light in the mid-infrared (MIR) spectral band has been very attractive owing to the various intriguing applications in a number of aspects, such as optical sensing, thermal imaging, biomedicine, free-space communications, etc [6]. Particularly, for modern optical communication, the two atmospheric transmission windows (3-5 and 8-14 μm) are included in the MIR band. On other hand, optical waveguides are basic components for integrated photonics. Such structures confine light propagation in reduced volumes, reaching high optical intensities of light. The performance of the bulk materials might be enhanced, and some applications could be realized in chip-scale wafers based on waveguides. In the MIR regime, waveguide structures have been achieved in silicon-on-insulator [7,8], silica on silicon [9], and chalcogenide glass [10] etc.

As one of the most efficient techniques for three-dimensional (3-D) volume micro-structuring of transparent dielectrics, the femtosecond (fs) laser inscription has been widely applied to fabricate optical waveguides in numerous optical materials, including optical crystals [11–14], ceramics [15–18], glasses [19–21], and polymers [22]. When an intense fs laser beam is focused inside a transparent crystal, some controlled micro-modifications occur

#185234 - $15.00 USD Received 11 Feb 2013; revised 9 Mar 2013; accepted 9 Mar 2013; published 13 Mar 2013

in the focal volume. Concerning the optical properties, in most of the crystals, the fs laser induces a reduction of the refractive index in the focal volume [23]. The most general way to fabricate waveguides in crystals is the so-called Type II approach: the fs laser creates severe damage tracks inside the bulk at the focal volume in which the refractive index decrease [24], but in the surrounding area the refractive index increases due to the stress induced effect [25]. To increase the refractive index contrast, two parallel irradiations are performed with a spatial separation of around 15-20 μm: the waveguide core is then in the region between the two damaged lines. Depressed cladding waveguide is another type of fs-laser inscription technique. It consists of a large number of low-index damage tracks, and the waveguide core results in the region surrounded by these tracks. Theoretically, the shape and size of the cladding structure could be adjusted with more flexibility [26–28]. Such structures have been realized in Nd or Tm doped YAG ceramics or crystals, Nd:YVO_4, BiB_3O_6 and $KTiOPO_4$ crystals [29–33]. As an obvious advantage over the Type II waveguides, large diameter of cladding waveguide enables them to guide light till longer wavelength regions. Particularly, multi- and single- mode cladding waveguides at MIR wavelengths fabricated by fs laser inscription in Tm:YAG have been reported [29].

The ZnS crystal is one of the most promising materials with a wide range of applications. It is also an excellent optical material for using in MIR waveguide devices due to its high refractive index (~2.2523 at the wavelength of 4 μm) and huge transparency window covering from visible to infrared wavelengths (0.37~14 μm) [34]. As of yet, there has not report on the waveguide fabrication in ZnS bulk crystals.

In this work, we report, to our best knowledge for the first time, on the fabrication of depressed optical cladding waveguides in ZnS crystal by the fs laser inscription. The guiding properties of the ZnS waveguides are investigated at the MIR wavelength of 4 μm.

2. Experimental

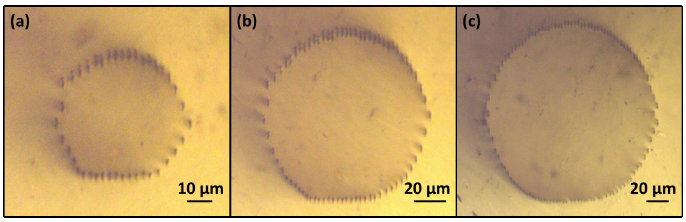

Fig. 1. Cross section of WG1 (a), WG2 (b) and WG3 (c) fabricated in ZnS crystal. The picture was taken with an optical microscope in transmission illumination.

The ZnS crystal was cut to the dimensions of 7.0 (x) × 10 (y) × 2.0 (z) mm^3, and the largest and the two edge faces of the sample were optically polished. An amplified Ti:Sapphire laser system, which delivered 120 fs pulses, linearly polarized at 800 nm, with a repetition rate of 1 kHz and 1 mJ maximum pulse energy, was employed to fabricate the depressed cladding waveguide structure at the Universidad de Salamanca, Spain. The sample was fixed on a motorized 3-axes stage that was moved at a constant velocity (500 μm/s) along the y direction of the sample. The laser beam, whose pulse energy was set to 2.5 μJ with the help of a calibrated neutral density filter and a half-wave plate, was focused through a microscope objective (Leica 40 ×, numerical aperture N.A. = 0.65) at a maximum depth of 125 μm beneath the surface. The selected pulse energy was chosen after multiple trials as a compromise between producing strong enough damage tracks, and avoiding the internal fracture of the sample. In order to produce the depressed cladding waveguides (WG 1~3, shown in Fig. 1, with diameter (D) ≈50 μm, 100 μm, 150 μm, respectively) multiple parallel scans of the sample were done with a lateral separation of 3 μm, following the desired circular geometry, from bottom to top of the structures.

One of the main difficulties for the fabrication of large core optical waveguides in ZnS is the strong spherical aberration [35] that is produced in the air-crystal interface due to the large

#185234 - $15.00 USD Received 11 Feb 2013; revised 9 Mar 2013; accepted 9 Mar 2013; published 13 Mar 2013

value of the refractive index. The chromatic aberration causes a very different energy distribution in the focal region for different focusing depths, and it requires the use of pulse energies in a relative narrow range in order to produced enough damage in all the laser tracks but avoiding the fracture of the sample: the selected pulse energy (2.5 μJ) is in such range for our experimental conditions. For such energy, the produced damage tracks are remarkably shorter than those produced in other crystals at similar scanning velocity.

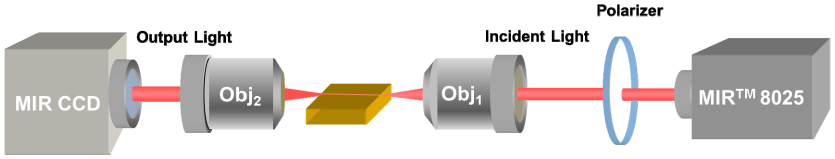

Fig. 2. Schematic of the end-face coupling arrangement applied to investigate the optical properties of the cladding waveguides in ZnS crystal.

The end-face coupling arrangement, shown in Fig. 2, was applied to investigate the near-field modal profiles of the depressed cladding waveguides and to determine the value of the maximum refractive index contrast in order to reconstruct the refractive index distributions. The incident light at 4 μm was generated in the Tunable Laser System - MIR^{TM} 8025 (Daylight Solutions, Inc.). The sample was mounted on a 6-D optical stage. The TE or TM polarized light of 4 μm was focused by a MIR microscope objective lens (ZnSe, LFO-5-12-3.75, N.A. = 0.13) to be coupled into the depressed cladding waveguides, and another MIR microscope objective lens was utilized to collect the output light at the other facet of the sample. A MIR CCD camera was employed to map the coupled light from the depressed cladding waveguide structure. Consequently, the near-field modal profile of the structure was obtained experimentally. We also measured the N.A. of the waveguide in order to get the maximum value of refractive index changes of the waveguide, by adjusting the position of the incident coupled light. In addition, the cross section of the waveguides was imaged by an optical microscope (Axio Imager, Carl Zeiss) operating in transmission mode.

3. Results and discussion

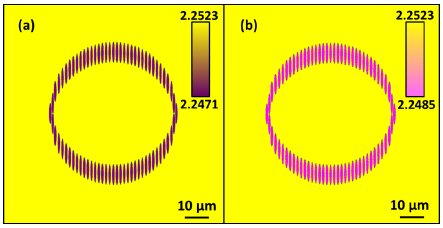

Fig. 3. The reconstructed refractive index profiles for the TE (a) and the TM (b) polarizations are shown.

In Fig. 1(a) we show the transverse section of WG1 (D ≈50 μm) taken with an optical microscope. The refractive index distribution of the depressed cladding waveguides cannot be directly measured by conventional measuring methods, such as the m-line technology. However, we can obtain indirectly the maximum value of the refractive index contrast between the low-index tubular cladding structure and the core waveguide region by measuring the N.A. of the waveguide, which could be roughly approximated by using the formula

$$\Delta n \approx \frac{\sin^2 \theta_m}{2n} \qquad (1)$$

where θ_m is the maximum incident angular deflection at which no transmitted power is detected, while n is the refractive index of the substrate [33]. The angle θ_m was measured by the modified end-face coupling arrangement in which a large YAG ceramic cuboid, used to

#185234 - $15.00 USD Received 11 Feb 2013; revised 9 Mar 2013; accepted 9 Mar 2013; published 13 Mar 2013

change the angle of the incident light, was added between the polarizer and the incident objective. Based on the measured θ_m we estimated the refractive index contrast of the depressed waveguide WG1 for the two transverse polarizations to be $\Delta n_{TE} \approx -5.2 \times 10^{-3}$ and $\Delta n_{TM} \approx -3.8 \times 10^{-3}$. Figures 3(a) and 3(b) show the reconstructed refractive index distributions. The two profiles, obtained from RSoft© software [36], show that the change of the refractive index for the TE polarization is larger than the one for the TM polarization.

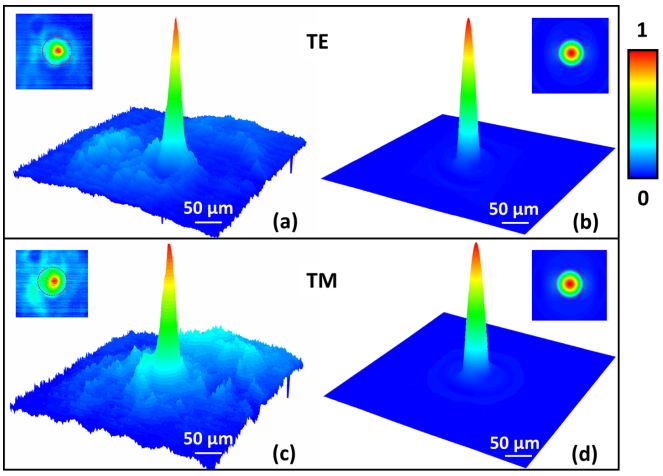

Fig. 4. 2-D, 3-D measured near-field modal profiles of WG1 for the TE (a) and TM (c) polarization, and calculated ones for the TE (b) and TM (d) polarization (The red circles in all the 2-D figures represent the position of the depressed cladding structure).

According to the reconstructed refractive index profiles, the 2-D and 3-D modal profiles of fundamental TE and TM mode for WG1 were calculated by using the finite-difference beam propagation method (FD-BPM) of the RSoft© software, as depicted in the Figs. 4(b) and 4(d). As one can see, the 2-D and 3-D calculated modal profiles are in very good agreement with the 2-D and 3-D experimental results shown in the Figs. 4(a) and 4(c), respectively. It suggests that the simulations based on the reconstructed refractive index profile were successful. The red circles in all the 2-D figures represent the position of the depressed cladding structure. From the calculated and experimental near-field modal profiles, it is obvious that the light guided in the cladding structure of WG1 is single-mode.

The propagation losses of WG1 for the TE and TM polarizations were estimated by directly measuring the powers of the incident and output light through the waveguide. The propagation loss for the TE polarization is ~3.9 dB/cm, lower than that measured for the TM polarization (~4.1 dB/cm). Two possible factors might be responsible for such difference. The first one is that the TM polarization is parallel to the inscription direction of the fs laser and to the produced damage tracks: thus, the light with the TM polarization could leave out of the cladding waveguide structure easier than the light for the TE polarization in the areas with larger track separations. The second one is the difference between the refractive index contrast in the structures, that is larger for the TE polarization, and it may improve the confinement properties. Therefore, the waveguiding performance of the fabricated structures could be probably improved by the reduction of the filament separation, and by scanning the sample at lower speed during the fs inscription in order to increase the refractive index contrast. Both procedures may be helpful to reduce the propagation loss further.

#185234 - $15.00 USD Received 11 Feb 2013; revised 9 Mar 2013; accepted 9 Mar 2013; published 13 Mar 2013

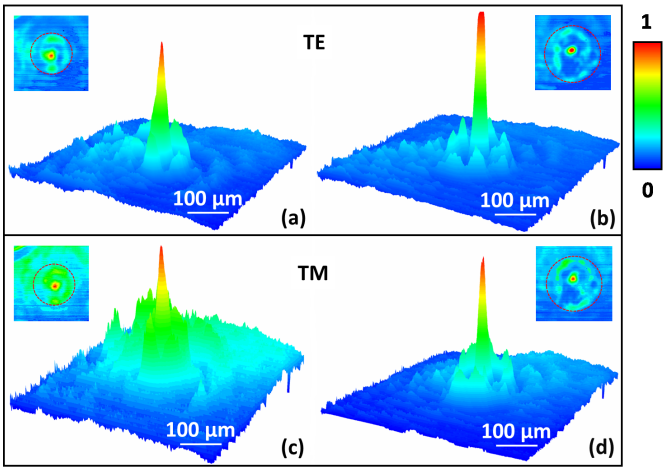

Fig. 5. 2-D, 3-D measured near-field modal profiles of WG2 for the TE (a) and TM (c) polarization, and the ones of WG3 for the TE (b) and TM (d) polarization (The red circles in all the 2-D figures represent the position of the depressed cladding structure).

In further investigation on the cladding waveguides, we found that, WG2 (D ≈100 µm) and WG3 (D ≈150 µm) with larger diameters are multimode for both TE and TM polarizations, as shown in Fig. 5. And the minimum propagation losses of the two waveguide structures are ~1.1 dB/cm for the TE polarization and ~1.3 dB/cm for the TM polarization, lower than those of WG1. In modern MIR optical communication, low-loss single-modal fibers are used more widely owing to the intermodal dispersion of multimode light. So this single-mode optical waveguide with the optimum size could be thus a promising fiber-coupling device in the future. However, due to the length of the damage tracks, the cladding waveguides cannot be fabricated with an arbitrarily small size and, moreover, small diameter cladding waveguides typically show larger propagation losses.

4. Summary

We have reported the fabrication of depressed cladding waveguides in ZnS crystal by using femtosecond laser inscription. The guiding properties in the MIR (wavelength 4 µm) have been investigated, showing very good performances, with single mode and multi-mode behavior for both TE and TM polarizations. The minimum propagation losses were measured at this wavelength resulting in ~1.1 dB/cm for the TE polarization and ~1.3 dB/cm for the TM polarization.

Acknowledgments

The work was supported by the National Natural Science Foundation of China (No. 11274203) and the Spanish Ministerio de Ciencia e Innovación (Projects CSD2007-00013 and FIS2009-09522), and Junta de Castilla y León (Project SA086A12-2).

#185234 - $15.00 USD Received 11 Feb 2013; revised 9 Mar 2013; accepted 9 Mar 2013; published 13 Mar 2013